ELSEVIER

Journal of Neuroscience Methods 165 (2007) 270–286

JOURNAL OF NEUROSCIENCE METHODS

www.elsevier.com/locate/jneumeth

Methods for quantifying intra- and inter-subject variability of evoked potential data applied to the multifocal visual evoked potential

Sangita Dandekar[a,*], Justin Ales[a], Thom Carney[a,b,c,d], Stanley A. Klein[a,b,c,d,e]

[a] *Vision Science Graduate Program, University of California, 360 Minor Hall, School of Optometry, UC Berkeley, CA 94720-2020, United States*
[b] *Helen Wills Neuroscience Institute, University of California, Berkeley, United States*
[c] *School of Optometry, University of California, Berkeley, United States*
[d] *Neurometrics Institute, Oakland, CA, United States*
[e] *Department of Bioengineering, University of California, Berkeley, United States*

Received 14 April 2007; received in revised form 12 June 2007; accepted 13 June 2007

Abstract

Differences in cortical geometry within and between subjects can complicate multifocal visual evoked potential (mfVEP) and standard evoked potential (EP) intra- and inter-subject comparisons. We present methods for aligning temporal intra- and inter-subject data prior to comparison.

Multiple groups have informally observed that the two dominant temporal principal components (PCs) of the pattern reversal visual evoked potential (VEP) obtained with singular value decomposition (SVD) exhibit little inter-subject variability relative to the inter-subject variability of the raw VEP. We present methods that employ the temporal PCs to formally quantify intra- and inter-subject variability of the mfVEP.

When SVD was applied to data from eight subjects separately, it was found that two PCs accounted for, on average, 73% of intra-subject variance. When a single SVD was applied to combined data from multiple subjects, it was found that two PCs accounted for 67% of inter-subject variance. We used the 2D temporal subspaces derived from SVD as a basis for intra- and inter-subject comparisons.

Keywords: EEG; Intra-subject variability; Inter-subject variability; Multifocal visual evoked potential; Evoked potential; Principal component analysis; Cortical folding

1. Introduction

Multiple groups including Maier et al. (1987), James (2003), Zhang and Hood (2004b), and Carney et al. (2006) have applied principal component analysis (PCA) via singular value decomposition (SVD) to either the conventional or the multifocal pattern reversal VEP and demonstrated in both cases that two principal components (PCs) account for a substantial amount of intra-subject variance. Several groups including (Maier et al., 1987; Zhang and Hood, 2004b) have also made the informal qualitative observation that the inter-subject variability of the two dominant, individually determined temporal principal components is considerably less significant than the inter-subject variability of the unprocessed VEP temporal waveforms. In this paper we use the subspaces derived from SVD to facilitate intra- and inter-subject comparisons of the multifocal VEP (mfVEP).

Although there are inter-subject similarities in the structural organization of human early visual areas, the folded shape of cortex is highly variable across subjects. The variability in the cortical folding patterns of human primary visual areas has been observed using functional magnetic resonance imaging (fMRI) in conjunction with structural MRI and retinotopic mapping techniques (DeYoe et al., 1996; Engel et al., 1997). The variability in the folding patterns of cortex in human visual areas has also been noted in VEP studies (Foxe and Simpson, 2002; Maier et al., 1987; Zhang and Hood, 2004b).

One likely manifestation of the inter-subject variability of cortical folding that is of particular interest in VEP studies (and EP studies in general) is the contribution of the variability of cortical folding to the observed inter-subject variability of voltage distributions on the scalp when subjects are presented with the same stimulus. Recent fMRI work by Bartels and Zeki (2004) implies that the underlying time courses of activation in response to visual stimuli associated with corresponding functional subdivisions of visual cortex might be expected to display significant inter-subject correlation. In VEP studies, even if the underlying

* Corresponding author. Tel.: +1 510 643 7571; fax: +1 510 643 5109.
E-mail address: sdandekar@berkeley.edu (S. Dandekar).

0165-0270/$ – see front matter © 2007 Elsevier B.V. All rights reserved.
doi:10.1016/j.jneumeth.2007.06.010

time courses of sources in visual cortex are the same across subjects, the inter-subject variability of cortical folding results in a unique linear combination of the source waveforms at the recording electrodes for every subject. The specific superposition of sources observed for a subject is significantly influenced by the specific cortical folding pattern of that individual. The inter-subject variability of cortical geometry is therefore a contributor to the inter-subject variability of the observed temporal potential waveforms on the scalp in VEP and other evoked potential studies.

Similar complications make intra-subject comparisons of mfVEP data difficult. The small, independently modulated patches used in mfVEP studies evoke activity in smaller regions of cortex than the conventional VEP (Baseler et al., 1994; Baseler and Sutter, 1997; Slotnick et al., 1999). The mfVEP data of a single subject has therefore been found to display considerable variability across the visual field simply due to local differences in cortical geometry (Baseler et al., 1994). It is therefore difficult to determine what fraction of intra-subject variability across the visual field is due to local differences in cortical geometry and what portion of the variability might be due to local differences in neural processing.

In this paper, we quantify intra- and inter-subject similarity of the time course of activation in early visual areas in response to pattern reversal. We employ the mfVEP to attempt to isolate the pattern reversal response in early visual areas. The mfVEP has been shown to minimize the contribution of extrastriate sources relative to the conventional, full field VEP when the mfVEP is presented at a sufficiently high frame rate (Fortune and Hood, 2003). The conclusion in Fortune and Hood (2003) was inferred from the observation of polarity reversal between the waveforms associated with the upper and lower visual hemifields in cases of relatively high frequency mfVEP stimulation bore closer resemblance to the waveforms that one might expect from striate generators (that should display such a polarity reversal) than did the polarity reversals observed in lower frequency mfVEP stimulation and the polarity reversals between the upper and lower fields observed with a conventional VEP stimulus.

As discussed, comparison of raw temporal data can be difficult largely due to cortical geometry differences. We apply SVD to reduce the dimensionality of both intra- and inter-subject mfVEP data and methods that operate on the data with reduced dimensionality to facilitate intra- and inter-subject comparisons.

2. Methods

2.1. Data collection/stimulus

Data were collected from eight subjects. The study was approved by the University of California, Berkeley, Committee for the Protection of Human Subjects and all subjects gave written informed consent prior to the beginning of experimentation. The subjects consisted of six males and two females. All subjects had normal or corrected-to normal vision. A mfVEP paradigm as developed and described by Sutter (1991) was used.

The stimulus consisted of 48 checkerboard patches arranged in 4 concentric rings (see Fig. 1). The unstimulated, inner diameter of the stimulus subtended 2.4°. The diameters of the four rings were 4.3°, 7.0°, 11° and 16°. The stimulus was presented on a Hitachi CM8 12U monitor with background luminance of 2.9 candelas/m^2 and patch contrast of 99%. Mean patch luminance was 16 candelas/m^2.

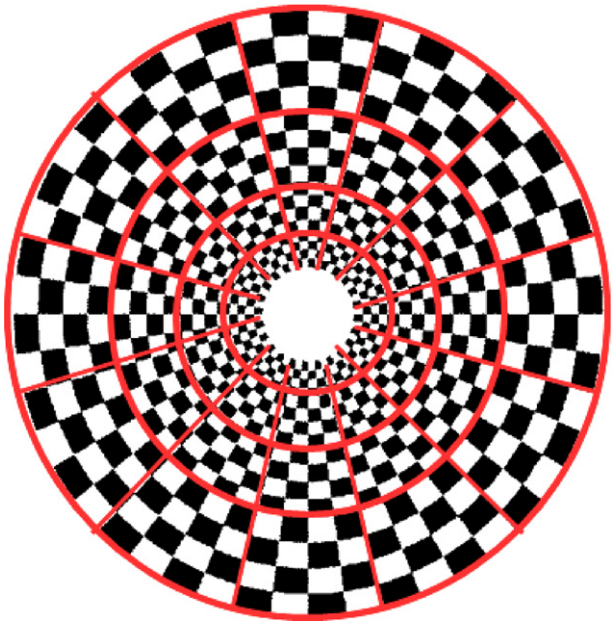

Fig. 1. mfVEP stimulus with 48 patches. To illustrate the stimulus each independently modulated patch is outlined in red. (No red lines were included in the stimulus when it was actually presented.) Stimulus diameter was 16° of visual angle. (For interpretation of the references to color in this figure legend, the reader is referred to the web version of the article.)

The stimulus was designed such that each patch activated approximately 64 mm^2 of visual cortex. Patch modulation was performed according to a binary, 16-bit *m*-sequence with a presentation rate of 60 Hz. The stimulus was presented using the WinVis psychophysical and physiological testing toolbox (www.neurometrics.com/winvis). Every subject participated in two to six runs of the sequence, with each presentation of the sequence lasting approximately 20 min. Each run was broken up into multiple 1 min segments. The multiple data runs from a single subject were averaged together. In analyses involving data from multiple subjects, only electrodes that displayed reasonable noise levels for all subjects were included. This procedure removed 23 electrodes from the multiple-subject analysis.

An ActiveTwo EEG system (www.biosemi.com) with 96 electrodes was used to sample scalp potentials at 512 Hz during stimulus presentation. The checkerboard reversal response (first cut of second order kernel, see Sutter, 1991 for details) was determined for each patch at each of the electrodes using the Fast-Walsh transform. The resulting data could be expressed as a function of three variables, $V(e, p, t)$, where e is the recording electrode (ranging from 1 to 96), p the stimulus patch (ranging from 1 to 48), and t is a time index.

A filter with a passband of 2–100 Hz was applied to the data. In addition, an average reference was applied to every dataset. Differences in the time of presentation of each individual patch

due to the vertical screen raster delay were taken into account during pre-processing of data.

2.2. SVD of single and multiple subject data

Application of SVD to mfVEP data of a single subject was performed as follows. Prior to the application of a SVD to single subject data, the $V(e, p, t)$ data from each subject was appropriately redistributed into a 2D matrix with $(E \times P)$ rows and N columns. P and E are the total number of patches and electrodes, respectively, and N denotes the total number of time samples over which the SVD was computed. All SVDs discussed in this paper were applied over the same time window in the pattern reversal response. Each time window consisted of 121 samples, corresponding to 37–260 ms after pattern reversal. Let us suppose that the SVD expansion has D dominant components(c) so that the original data set can be approximated by the expansion:

$$V(e \times p, t) \cong \sum_{c=1}^{D} E(e \times p, c)T(c, t) \tag{1}$$

(The SVD diagonal eigenvalue matrix is multiplied by the left-most matrix of the SVD to form the E matrix above.) Note that if the data is full rank, when D equals the total number of time points, N, the expansion shown in Eq. (1) is equivalent to the original data.

A similar application of SVD was applied to data from all eight subjects grouped together. In the case of data from multiple subjects, the data was grouped into a 2D matrix with $(S \times E \times P)$ rows and N columns, where S is the number of subjects and E, P and N are defined as above. Similar to the individually applied SVD, an approximation of the multiple subject data using the first D dominant components of the SVD can be written as:

$$V(s \times e \times p, t) \cong \sum_{c=1}^{D} E(s \times e \times p, c)T(c, t) \tag{2}$$

The expansions in Eqs. (1) and (2), can be used to write the fraction of variance accounted for either by the individual subject expansion (varI) or by the expansion for data from all subjects combined (varA):

$$\text{varI} = \frac{\sum_{e,p,t}\left(\sum_{c=1}^{D}(E(e \times p, c)T(c, t))^2\right)}{\sum_{e,p,t}\left(\sum_{c=1}^{N}(E(e \times p, c)T(c, t))^2\right)} \tag{3}$$

$$\text{varA} = \frac{\sum_{s,e,p,t}\left(\sum_{c=1}^{D}(E(s \times e \times p, c)T(c, t))^2\right)}{\sum_{s,e,p,t}\left(\sum_{c=1}^{N}(E(s \times e \times p, c)T(c, t))^2\right)} \tag{4}$$

The simplicity of these two equations is a result of the orthogonality of the various terms in the SVD expansion. (It should be noted that an alternative, easily applied method to calculate the percent variance accounted for by some subset of the principal components is to determine the ratio of the sum of the squares of the eigenvalues associated with the PCs of interest to the sum of the squares of all eigenvalues. See Zhang and Hood, 2004b.)

A main motivation for this paper is the empirical finding that Eq. (4) provides almost as good a fit to the raw data as Eq. (3). As will be discussed further in Section 3, it was found that for $D = 2$ the percent of the variance accounted for by Eq. (4) (varA = 67%) is almost the same as for Eq. (3) (varI = 73%). We consider this minor reduction in variance to be remarkable because Eq. (2), the expansion of data from multiple subjects, involves eight times ($S = 8$) the number of data points as the single subject case.

2.3. Comparison of 2D subspaces

The findings that varI was 73% on average for each subject and varA was 67% as defined in Eqs. (3) and (4) indicate that both intra- and inter-subject data were well-described by 2D subspaces.

These results suggest that temporal inter- and intra-subject comparisons could be simplified by comparing the 2D temporal subspaces derived from SVD of the data (i.e. $T(c, t)$ for $c = 1$–2 in Eq. (1) for intra-subject comparisons and $T(c, t)$ in Eq. (2) for $c = 1$–2 in Eq. (2) for inter-subject comparisons). It should be noted that the methods to be presented for comparisons of 2D subspaces could also be extended to subspaces derived from EEG data with dimensionality greater than two.

Prior to applying SVD according to the procedures described in Section 2.2, the data were transformed to have zero mean across each temporal observation/time dimension. At every time point, the mean across waveforms at that time point was subtracted. This step ensured that the temporal PCs resulting from different applications of SVD had minimal DC offsets from one another.

For the intra-subject comparisons, we compared temporal subspaces that were derived from SVD applied to different subsets of the visual field for the same subject. The mfVEP data for a single subject demonstrates differences in local folding patterns of cortex across the visual field as well as possibly different responses due to functional differences across the visual field (Baseler and Sutter, 1997). However, it has been shown that patches at the same eccentricity of the mfVEP display relatively similar temporal responses (Baseler and Sutter, 1997). SVDs were therefore applied to subsets of patches from the same eccentricity (i.e. one SVD for each concentric ring of the stimulus, applying Eq. (1) to only the appropriate subset of patches corresponding to each ring). Four SVDs, one for each stimulus ring, were therefore applied to data from each subject. This resulted in four 2D subspaces per subject.

2.4. Use of composite subspace as reference plane for comparisons

Rather than comparing each of the four intra-subject temporal 2D subspaces (which will be referred to as "individual" subspaces and be denoted as $I(c, t)$) to all other intra-subject subspaces for the same subject, we defined what we shall refer to as a 'composite' subspace. We shall denote the composite subspace as $C(c, t)$. It was determined by applying the decomposition in Eq. (1) to data from the entire field from each subject. The composite plane served as a fixed reference to which other data could

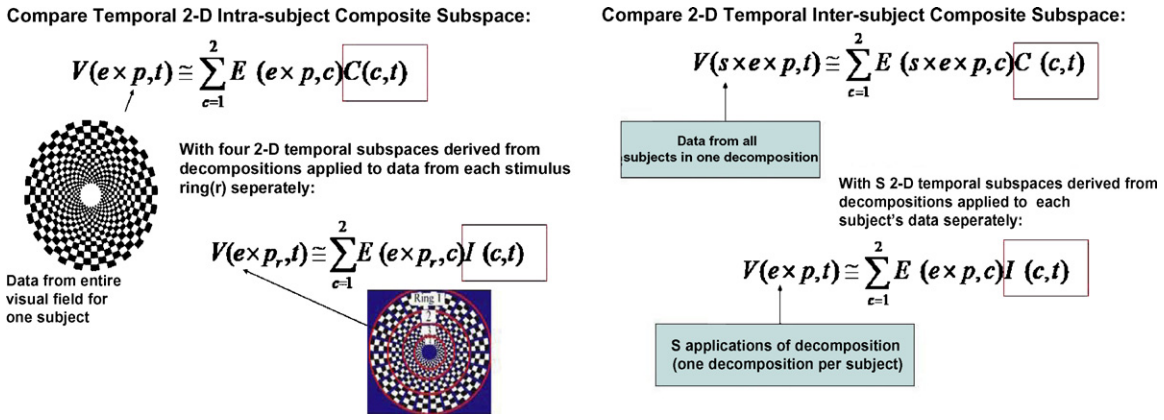

Fig. 2. Left side: illustration of methods for intra-subject comparisons. Comparisons for a single subject are performed by applying SVD to data from the entire visual field for a single subject and comparing the resulting 2D temporal "intra-subject composite" subspace with the 2D "individual" subspaces resulting from application of SVD to each of the stimulus rings separately. Right side: similar to left side except showing methods for inter- rather than intra-subject comparisons.

be compared. Intra-subject comparisons were between the intra-subject $C(c, t)$ subspace and the four "individual" intra-subject $I(c, t)$s. Fig. 2 (left) illustrates the subspaces used in intra-subject comparison.

Similarly, for inter-subject comparisons, we could compare an inter-subject composite, $C(c, t)$, that was determined via decomposition of data grouped from the multiple subjects (as shown in Eq. (2)), to decompositions applied to data from each subject individually (resulting in "individual" subspaces, $I(c, t)$). Use of a composite subspace in the inter-subject comparisons avoided having to perform a pair-wise comparison for each of the eight single subject subspaces. Fig. 2 (right) illustrates the subspaces used in inter-subject comparisons.

2.5. Intra- and inter-subject comparisons and the rotation problem

The "rotation problem" of SVD complicates intra- and inter-subject comparisons. Even if there are similar underlying temporal processes in response to pattern reversal across the visual field within a single subject, or temporal similarities between subjects, distortions due to differences in cortical geometry within a subject and between subjects are expected to cause the SVD components (as well as the raw EEG data) to be some unknown linear combination of the true sources (see Appendix A.1 for a simulated example of how cortical folding affects the SVD time functions).

Determining the degree of similarity of $C(c, t)$ and any given individual subspace, $I(c, t)$, is therefore complicated by the rotation problem. In order to address the problem, a method is developed that searches for the linear combination of sources in each $I(c, t)$ that is most similar to the rotation in $C(c, t)$. The motivation for comparing similar linear combinations of sources is to obtain improved quantitative comparison metrics. Improved comparison metrics are expected to result from examining comparable linear combinations of sources so that differences that are likely due to cortical geometry can be identified.

Methods to find linear combinations of sources in individual subspaces that best correspond to those in a composite subspace and accompanying methods to quantify similarity are formally developed in Section 2.6. In this section, we present an example to clarify the motivation for the methods presented in Section 2.6.

Fig. 3 contains simulated data that illustrates how the rotation problem could complicate comparisons by masking similarities between two sets of EEG signals. Fig. 3 illustrates two dominant temporal vectors in a composite subspace (shown in blue). We shall denote the first temporal PC associated with a composite subspace as $C(1, t)$ and the second temporal principal component associated with a composite as $C(2, t)$. The two, dominant temporal PCs defining an individual subspace that we wish to compare to the composite subspace will be denoted as $I(1, t)$ and $I(2, t)$, respectively (shown in red in Fig. 3). It can be seen that

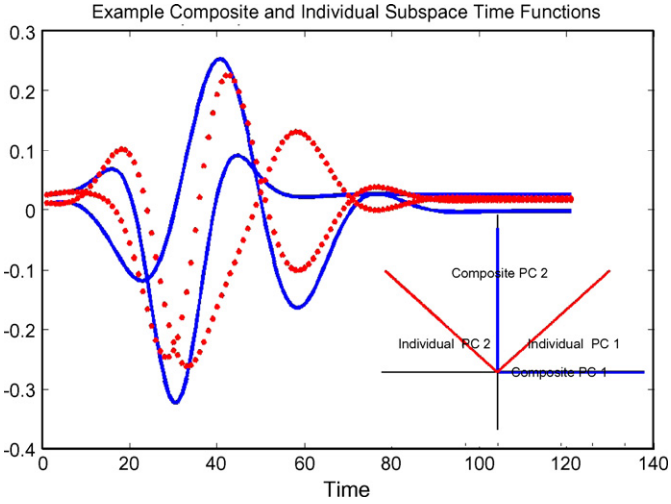

Fig. 3. Simulated data to illustrate rotation problem. Two composite subspace PCs (blue) and two individual subspace PCs (red) appear, at first glance, to differ. However, any rotation/linear combination of sources in the composite subspace (as determined by value of θ in Eq. (5)) can be matched exactly by a rotation in the in the individual subspace (ϕ_i in Eq. (6)) so that $C'(t, \theta) = I'_m(t, \phi_i)$. Inset: illustration of both pairs of PCs in their shared 2D subspace. Note that the individual subspace (red) can be rotated within the shared 2D subspace into alignment with any in-plane rotation of the composite subspace (blue). (For interpretation of the references to color in this figure legend, the reader is referred to the web version of the article.)

the two sets of two dominant PCs in Fig. 3 look substantially different at first glance.

Rotations in the composite plane can be specified relative to the unrotated composite vector $C(1, t)$ (with a rotation of $\theta = 0$ corresponding to being perfectly aligned with ($C(1, t)$ and a rotation of $\theta = 90$ corresponding to $C(2, t)$). The rotations are determined via Eq. (5):

$$C'(t, \theta) = C(1, t)\cos(\theta) + C(2, t)\sin(\theta) \tag{5}$$

Similarly, rotations in an individual subspace are measured relative to a rotation of $\phi_i = 0$ that corresponds to $I(1, t)$. The rotations in the individual subspace can be written as:

$$I'(t, \phi_i) = I(1, t)\cos(\phi_i) + I(2, t)\sin(\phi_i) \tag{6}$$

Although the simulated data in Fig. 3 appears to exhibit differences between C and I, every rotation/linear combination in the composite space is matched perfectly by some other linear combination of sources in the individual subspace. The result is due to the fact that, in the simulated data, the individual subspace and the composite subspace are identical with the exception that the $I(1, t)$ and $I(2, t)$ vectors that define the individual subspace are rotated in the shared subspace by $\pi/4$ relative to $C(1, t)$ and $C(2, t)$. Thus, for example, a rotation corresponding to $\theta = 0$ according to Eq. (5) such that $C'(t, \theta) = C(1, t)$ can be matched by evaluating Eq. (6) with $\phi_i = -\pi/4$ so that the time function at the rotation θ in the composite subspace equals the time function at the rotation ϕ_i in the individual subspace, i.e. $C'(t, \theta) = I'_m(t, \phi_i)$.

The simulated data highlights the importance of comparing corresponding linear combinations of sources in EEG data. If corresponding linear combinations of sources are not compared, differences that are simply due to a different superposition of sources might be confused with differences of genuine interest.

In the simulated data, the individual and the composite subspace were identical. If the subspaces under comparison aren't identical a question of interest is whether or not the subspaces under comparison possess similar linear combinations of sources. Also of interest is quantifying the extent of the observed similarity. A comparison metric employed in Section 2.6 for comparisons of multiple individual subspaces is how similar all individual subspaces are at the linear combination of PCs that is most similar among all of the individual subspaces. The linear combination of PCs displaying the greatest similarity to all of the subspaces under comparison will be denoted as $C'(t, \theta_{\max})$. The $C'(t, \theta_{\max})$ could indicate a neural process that is shared between all of the sets of EEG data that are under comparison. Also of interest is the linear combination of PCs that displays the greatest differences between the individual subspaces under comparison, which will be denoted as $C'(t, \theta_{\min})$. The $C'(t, \theta_{\min})$ could indicate a neural process that is relatively variable in the sets of EEG data under comparison. It should be noted that the maximum and minimum similarity metrics presented in Section 2.6 can be extended to subspace comparisons of higher dimensions than two. The methods we present for $N = 2$ dimensional subspace comparisons consist of a search for maxima and minima over one $(N - 1)$ free rotation parameter. To extend this to a general N-dimensional subspace comparison, one could search for maxima and minima over $N - 1$ rotation parameters.

2.6. Methods for intra- and inter-subject comparison

Given any linear combination of sources in the composite subspace, the corresponding rotation in an individual subspace with the greatest similarity to those sources in the composite plane can be determined.

The composite is used as a reference that allows similar linear combinations of sources in multiple individual subspaces to be compared. The metric used to quantify similarity between the composite and any given individual subspace is the sum-squared error (SSE).

If one fixes the rotation in the composite subspace at θ, the θ will specify a single linear combination of sources in the composite plane. One can then determine the particular rotation in an individual subspace (ϕ_{irot}) that minimizes the SSE between the $I'_m(t, \phi_i)$ and the $C'(t, \theta)$ (see Eqs. (5) and (6) for definitions of $C'(t, \theta)$ and $I'_m(t, \phi_i)$):

$$\phi_{\text{irot}} = \underset{\phi_i}{\operatorname{argmin}} \sum_{t=1}^{N} (C'(t, \theta) - I'_m(t, \phi_i))^2 \tag{7}$$

Because both $I'_m(t, \phi_i)$and $C'(t, \theta)$ are unit length:

$$\begin{aligned} \phi_{\text{irot}} &= \underset{\phi_i}{\operatorname{argmin}} \sum_{t=1}^{N} (-2C'(t, \theta) I'_m(t, \phi_i)) \\ &= \underset{\phi_i}{\operatorname{argmax}} \sum_{t=1}^{N} (C'(t, \theta) I'_m(t, \phi_i)) \end{aligned} \tag{8}$$

From Eq. (8) it can be seen that finding the rotation in an individual subspace that minimizes the SSE between it and any given rotation in the composite plane can be found by maximizing the dot product of $I'_m(t, \phi_i)$ and the $C'(t, \theta)$. If θ is fixed, the ϕ_i that maximizes the dot product of $I'_m(t, \phi_i)$ and the $C'(t, \theta)$ is simply the ϕ_i where $C'(t, \theta)$ projects onto the individual subspace.

Projection length will be extensively used as a metric for similarity. The reader should keep in mind the result of Eqs. (7) and (8) that minimizing the SSE is equivalent to maximizing projection length.

Therefore, given a time function in the composite subspace at rotation θ corresponding to some linear combination of sources, $C'(t, \theta)$, the corresponding rotations in each of the individual subspaces that minimized the sum squared error with $C'(t, \theta)$ were found by projecting $C'(t, \theta)$ onto each individual subspace. This was done for all rotations in the composite subspace, θ. Fig. 4A is a synthetic example of the rotation of a vector, $C'(t, \theta)$ shown in red, within a composite subspace (shown in blue) in three time dimensions. Shown in black and shaded in gray is another 2D subspace embedded in 3D that could correspond to an individual subspace.

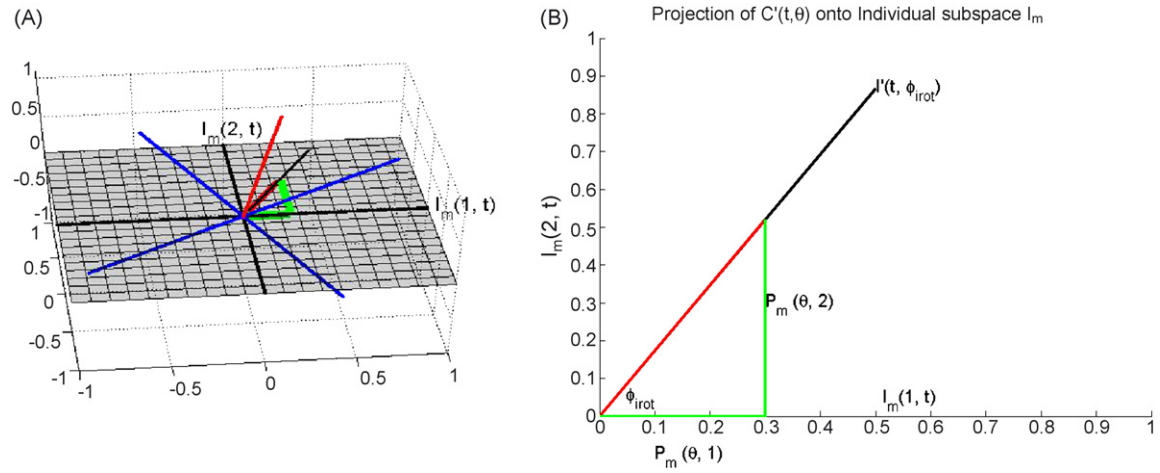

Fig. 4. (A) Synthetic 3D illustration of rotation $C'(t, \theta)$ in composite subspace. The subspace in blue is the composite subspace. The subspace in black that is shaded gray is an individual subspace with some tilt relative to the composite. The vector that is rotated in the plane of the composite subspace, $C'(t, \theta)$, is shown in red and the two components of the projection ($P_m(\theta, 1)$ and $P_m(\theta, 2)$) are shown in green. (B) Illustration of the projection of $C'(t,\theta)$ onto an individual subspace. The projection onto the subspace is shown in red. The two components of the projection are shown in green. The time function in the individual subspace at the location of the projection of $C'(t, \theta)$, $I'(t, \phi_{\text{irot}})$, is shown in black. ϕ_{irot} is as defined in Eq. (11). (For interpretation of the references to color in this figure legend, the reader is referred to the web version of the article.)

The two components ($c = 1$ and 2) of the projection of $C'(t, \theta)$ onto the mth individual subspace can be written as:

$$P_m(\theta, c) = \sum_{t=1}^{N} C'(t, \theta) \times I_m(c, t) \tag{9}$$

$P_m(\theta, 1)$ and $P_m(\theta, 2)$ are shown in green in Fig. 4A and B. Fig. 4B is an example of what the projection of the composite rotation onto the individual subspace might look like if the projection were viewed on the 2D individual subspace. It can be seen that length of the projection of the composite onto the mth individual subspace can be written as:

$$L_m(\theta) = \sqrt{P_m(\theta, 1)^2 + P_m(\theta, 2)^2} \tag{10}$$

Since all temporal waveforms were unit length (due to being derived from SVD and the rotation procedure being length-preserving) the maximum possible projection length of any rotation in the composite plane onto each individual subspace was one. A projection length of one is expected to occur if the two subspaces being compared are coplanar at a rotation in the composite subspace. Plots of $L(\theta)$ (i.e. plots of projection length onto an individual subspace versus rotation in the composite plane) are used extensively in Section 3 to compare intra- and inter-subject data. For a further description of the interpretation of these plots, see Appendix A.3.

It can be seen from Fig. 4B that the rotation of the projection of $C'(t, \theta)$ (specified within the mth individual subspace) can be expressed as:

$$\phi_{\text{irot}} = a\tan\left(\frac{P_m(\theta, 2)}{P_m(\theta, 1)}\right) \tag{11}$$

(For an alternative derivation of Eq. (11) that employs exclusively SSE rather than geometry, see Appendix A.2.) If the phase of a projection of a rotation in the composite plane onto an individual subspace fell in the left half of an individual subspace, the location of projection was rotated by 180° such that it was transformed to lie in the right half of an individual subspace. The rotation by 180° of projections in the left halves of individual subspaces was performed so that all phases could be easily compared to the positive, unrotated PC 1 in each individual subspace.

To find the rotation in the composite subspace, $\theta_{\max}$, that produces the greatest agreement between $C'(t, \theta)$ and the corresponding projections onto the multiple individual subspaces, one can find the θ that maximizes the sum of the lengths of the projections onto all of the individual subspaces. If M is the total number of individual subspaces, then $\theta_{\max}$ is as defined below:

$$\theta_{\max} = \underset{\theta}{\text{argmax}} \left(\sum_{m=1}^{M} \sqrt{P_m(\theta, 1)^2 + P_m(\theta, 2)^2} \right) \tag{12}$$

The time function in the composite plane located at the rotation $\theta_{\max}$, $C'(t, \theta_{\max})$, is expected to be a temporal source or combination of temporal sources that displays similarity in all individual subspaces.

Similarly the rotation in the composite plane that minimizes the sum of the lengths of the projections onto M individual subspaces is $\theta_{\min}$:

$$\theta_{\min} = \underset{\theta}{\text{argmin}} \left(\sum_{m=1}^{M} \sqrt{P_m(\theta, 1)^2 + P_m(\theta, 2)^2} \right) \tag{13}$$

The time function located at the rotation in the composite plane producing the minimum sum of lengths of projections onto the individual subject subspaces will be referred to as $C'(t, \theta_{\min})$.

The time functions in each of the individual subspaces at the rotations that are coincident with the projections of $C'(t, \theta_{\max})$ and $C'(t, \theta_{\min})$ onto each of the individual subspaces will be denoted as $I'_{\max}$ and $I'_{\min}$, respectively. The rotation angle

Table 1
SNRs across the visual field across subjects

Subject	Ring 1 (outer ring)	Ring 2	Ring 3	Ring 4 (fovea)	Entire visual field
1	2.6 ± 0.6	2.8 ± 0.8	2.7 ± 0.8	2.6 ± 0.6	2.7 ± 0.7
2	2.4 ± 0.7	2.1 ± 0.6	2.3 ± 0.9	2.4 ± 0.7	2.3 ± 0.7
3	1.8 ± 0.5	1.5 ± 0.3	1.4 ± 0.3	1.3 ± 0.2	1.5 ± 0.4
4	1.9 ± 0.3	1.9 ± 0.3	1.8 ± 0.4	1.7 ± 0.4	1.8 ± 0.4
5	1.9 ± 0.4	1.5 ± 0.3	1.5 ± 0.2	1.4 ± 0.2	1.6 ± 0.3
6	3.1 ± 0.8	2.4 ± 0.5	2.1 ± 0.5	2.1 ± 0.5	2.4 ± 0.7
7	3.6 ± 0.6	2.8 ± 0.4	2.4 ± 0.3	2.5 ± 0.5	2.8 ± 0.6
8	1.9 ± 0.3	1.4 ± 0.3	1.6 ± 0.4	1.8 ± 0.3	1.7 ± 0.4
Mean	2.4	2.1	2.0	2.0	2.1
S.E.	0.2	0.2	0.2	0.2	0.2

The standard deviation shown for each subject/ring combination is the standard deviation across the 12 patches composing each ring. The bottom row is the standard error across all subjects. It is given by the standard deviations of the SNRs of individual subjects divided by sqrt(8).

(as specified within an individual subspace) corresponding to the location of $I'_{\max}$ in the individual subspace will be denoted as $\phi_{i\,\max}$. The rotation angle (as specified within an individual subspace) corresponding to the location of $I'_{\min}$ in the individual subspace will be denoted as $\phi_{i\,\min}$.

The M $I'_{\max}$ in the M individual subspaces under comparison are expected to be linear combinations of sources in the individual subspaces exhibiting relatively great similarity. In contrast, the M $I'_{\min}$ in the compared individual subspaces are expected to be linear combinations of sources in the individual subspaces that exhibit relatively great variability.

3. Results

3.1. Subject signal to noise ratio

Signal to noise ratios (SNRs) were determined from each subject's $V(e, p, t)$ data using a method that was similar to the method presented in Zhang and Hood (2004a). Signal windows were defined as 37–260 ms (window length was 121 samples) after pattern reversal within the evoked response to each stimulus patch. The RMS amplitude of signal windows for each patch were used to calculate the SNR values shown in Table 1. The same method was used to determine RMS amplitudes in the "noise" regions of responses, defined as being 667–890 ms after pattern reversal in the evoked response to each stimulus patch. Noise window lengths were the same lengths as the signal windows, 121 samples. SNRs, the ratios between the two RMS measures in various regions of the visual field, are listed in Table 1 and discussed in later sections.

3.2. Intra-subject results

SVDs were performed on data from the entire visual field for each subject after forming a $V(e \times p, t)$ matrix for each subject as described in Section 2.2.

Table 2 lists the percent variance associated with the first four eigenvalues of each subject accounting for the most variance. Similar to the results found in Maier et al. (1987), James (2003) and Zhang and Hood (2004b), two principal components accounted for, on average for each individual subject, 73% of the total signal variance. This implies that, for every subject tested, the original VEP data can be well-approximated by the sum of products of two time dependent (T) and two spatial (E) components and that each subject's temporal data can be well-approximated by a 2D subspace.

As discussed in Section 2, each subject had an associated 2D "intra-subject composite subspace" determined by applying Eq. (1) to data from the entire visual field for each subject. In addition, four individual ring temporal subspaces were determined for each subject by applying Eq. (1) to data from each stimulus ring. Four $L(\theta)$ curves were determined for each subject as follows: a single vector was rotated within the composite subspace and at every rotation in the composite subspace the vector was projected onto each of the four individual subspaces corresponding to each stimulus ring for each subject (application of Eq. (10) at each θ from $-\pi/2$ to $\pi/2$). Each $L(\theta)$curve consisted of a plot of the projection length of the projection of the vector that was rotated in the composite subspace onto each individual subspace versus its rotation within the composite plane (see Section 2 and Appendix A.3 for more details). The sums of the $L(\theta)$ curves

Table 2
Percent variance accounted for by the first four PCs of intra-subject SVDs across the visual field

	Subject								Mean
	1	2	3	4	5	6	7	8	
% variance, PC 1	68	69	44	51	45	67	56	44	57
% variance, PC 2	14	13	12	18	13	20	24	26	18
% variance, PC 3	3.7	3.8	10	7.2	8.7	6.2	4.4	7.8	6.5
% variance, PC 4	3.8	2.9	7.9	5.9	6.5	2.4	3.6	5.6	4.8
PC1 + PC2	82	82	56	69	58	87	80	70	73

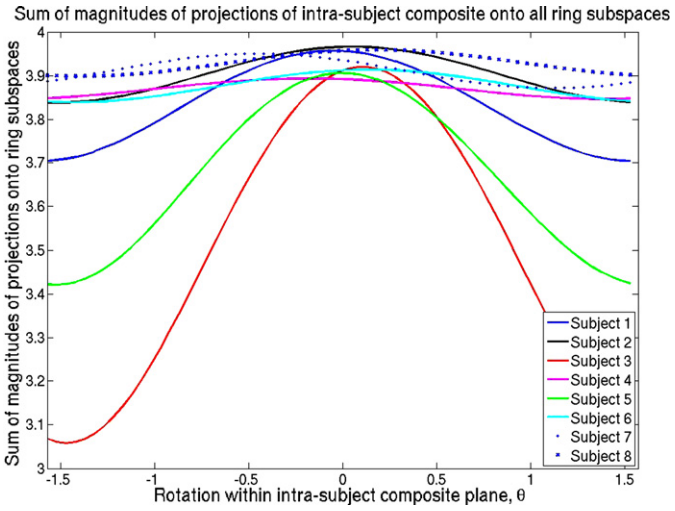

Fig. 5. Sum of $L(\theta)$ curves across four rings for each subject. Four $L(\theta)$ curves were determined (one per ring) according to Eq. (10) for each subject and then summed across the four-stimulus rings to create the curves above. Rotation within the intra-subject composite plane is specified relative to the unrotated principal component 1 in the composite plane. If the value of the sum of projections onto all ring subspaces was four for all rotations within the composite plane, it would indicate that each of the four ring subspaces was identical.

across all four rings for each of the subjects are shown in Fig. 5. If the 2D subspaces associated with all four rings of a subject's data were located in the same subspace as the intra-subject composite, the sum of the projection lengths at each rotation of the intra-subject composite would be four (sum of four unit length projections onto four ring subspaces). The sum of $L(\theta)$ curves for some subjects can be seen to deviate more substantially from four and therefore display greater intra-subject variability than others, in particular the curves of subjects 3 and 5. Note in Table 2 that two components accounted for only 56% and 58% of the total variance for these two subjects. In addition, note that in Table 2 the ratio of the percent variance accounted for by PC 2 to the percent variance accounted for by PC 3 is significantly smaller for subjects 3 and 5 than the same ratio as determined for the other subjects.

Subject 3 showed a sum of projection lengths that significantly deviated from four for most composite rotations. The low SNR of subject 3's data could be at least partially responsible for this result. Similarly, it is possible that some portion of the inconsistency between rings shown by subject 5 is attributable to effects of low SNR (see Table 1).

Several subjects displayed quite similar $L(\theta)$ curves for the subspaces derived from all four-stimulus rings with projection lengths uniformly near one for each stimulus ring. As can be seen in Fig. 5, even the minima of the sum of the four $L(\theta)$ curves for subjects 2, 4, 6, 7 and 8 are above 3.8, indicating a significant amount of similarity between each individual ring subspace and the intra-subject composite subspace at all rotations within the intra-subject composite plane. These results indicate that some or all of the sources contributing to the responses to the individual rings of the stimulus for these subjects were similar to one another.

Of interest is the rotation in the intra-subject composite subspace, $\theta_{\max}$, that maximized the sum of the lengths of the projections onto each of the individual ring subspaces via application of Eq. (12) across all four-stimulus rings for each subject. The $\theta_{\max}$ for each subject is shown in Table 3. The greatest projection lengths onto the individual ring subspaces were determined for each subject by plugging their particular $\theta_{\max}$ into Eq. (10), and are listed as "$L(\theta_{\max})$" in Table 3. The $L(\theta_{\max})$ indicates how similar the individual subspaces are at the rotations in each of the individual subspaces that make the individual time functions most similar. It can be seen that all of the $L(\theta_{\max})$ are relatively near the maximum possible value of one for all subjects and all stimulus rings. A possible interpretation of this result is that each of the $C'(t, \theta_{\max})$ represents a temporal neural process of substantial consistency across the visual field for each subject.

In order to determine which rotation in the intra-subject composite plane deviated the most substantially from the individual ring data, we could find the rotation in each intra-subject composite, $\theta_{\min}$, that minimized the sum of the lengths of the projections onto each of the individual ring subspaces via application of Eq. (13) across all four-stimulus rings for each subject. (Recall that this would be equivalent to finding the rotations in the individual subspaces that maximized the SSE between the individual subspaces.) The $\theta_{\min}$ are shown in Table 3. The projection lengths, $L(\theta_{\min})$, onto the individual ring subspaces as determined for each subject by plugging their particular $\theta_{\min}$ into Eq. (10), are also shown in Table 3.

It can be seen that the $L(\theta_{\min})$ are relatively near one for most subjects (however not as consistently near one as the $L(\theta_{\max})$). The projection lengths near one indicate that there was relatively

Table 3
The lengths of projection of $C'(t, \theta_{\max})$ and $C'(t, \theta_{\min})$ onto individual ring subspaces, $L(\theta_{\max})$ and $L(\theta_{\min})$, respectively

Subject	$\theta_{\max}$	$\theta_{\min}$	Ring 1 $L(\theta_{\max})$	Ring 1 $L(\theta_{\min})$	Ring 2 $L(\theta_{\max})$	Ring 2 $L(\theta_{\min})$	Ring 3 $L(\theta_{\max})$	Ring 3 $L(\theta_{\min})$	Ring 4 $L(\theta_{\max})$	Ring 4 $L(\theta_{\min})$
S1	.049	1.54	.986	.796	.995	.969	.995	.988	.981	.951
S2	−.050	1.52	.992	.955	.991	.983	.994	.946	.989	.954
S3	−.105	1.47	.995	.779	.993	.813	.969	.766	.962	.700
S4	.183	−1.38	.985	.907	.993	.994	.975	.987	.940	.958
S5	.003	1.53	.978	.667	.993	.923	.976	.915	.958	.916
S6	−.140	1.44	.995	.986	.995	.970	.978	.981	.946	.901
S7	.449	−1.12	.997	.989	.994	.982	.988	.970	.971	.931
S8	−.177	1.39	.987	.979	.991	.985	.995	.973	.987	.961

Table 4
Rotations in individual subspaces, $\phi_{i\,\max}$ and $\phi_{i\,\min}$, at locations of projection of intra-subject $C'(t, \theta_{\max})$ and $C'(t, \theta_{\min})$

Subject	$\theta_{\max}$	$\theta_{\min}$	Ring 1 $\phi_{i\,\max}$	Ring 1 $\phi_{i\,\min}$	Ring 2 $\phi_{i\,\max}$	Ring 2 $\phi_{i\,\min}$	Ring 3 $\phi_{i\,\max}$	Ring 3 $\phi_{i\,\min}$	Ring 4 $\phi_{i\,\max}$	Ring 4 $\phi_{i\,\min}$
S1	.049	1.54	−.197	1.34	.193	−1.39	.036	−1.51	.181	−1.33
S2	−.050	1.52	−.012	1.56	−.185	1.39	.108	−1.47	−.234	1.34
S3	−.105	1.47	.179	−1.41	−.146	1.43	.329	−1.29	.019	1.52
S4	.183	−1.38	.097	−1.48	.298	−1.27	.347	−1.22	.018	−1.56
S5	.003	1.53	−.119	1.33	−.036	1.50	−.215	1.24	.569	−.869
S6	−.140	1.44	−.099	1.48	−.123	1.42	−.376	1.22	.840	−.703
S7	.449	−1.12	−.376	1.19	−.541	1.01	−.280	1.26	1.46	−.143
S8	−.177	1.39	.466	−1.10	.673	−.898	−.518	1.04	−.283	1.27

little tilt/dissimilarity between each individual ring subspace and the composite subspace even at the $C'(t, \theta_{\min})$ rotation within the composite plane that minimized the sum of the lengths of the projections onto the individual subspaces. (See Appendix A.3 for a description of the meaning of 'tilt.') The main exceptions were subjects 1, 3 and 5 who, although they displayed $L(\theta_{\max})$ that were close to one, displayed significant deviations from unity in $L(\theta_{\min})$.

Table 4 lists the rotations within the individual ring subspaces, $\phi_{i\,\max}$, in radians at the location of projection of $C'(t, \theta_{\max})$ onto each ring subspace (Eq. (11) was applied to determine $\phi_{i\,\max}$ for each individual ring subspace for each subject). Fig. 6 is a plot of the projections of the each subject's $C'(t, \theta_{\max})$ onto the four ring subspaces of all eight subjects. The lengths and phases shown in Fig. 6 correspond to the actual rotations and lengths of the projections.

It can be seen from Table 4 and Fig. 6 that most of the rotations are closer to the unrotated PC 1 in each individual's subspace (defined as being at 0 phase within each individual subspace) than to the unrotated PC 2 in each individual's subspace (defined as being at $\pi/2$ phase within each individual subspace). However, there is a considerable deviation from the unrotated PC 1 in most cases.

Subjects 6 and 7, for example, both had $\phi_{i\,\max}$ associated with the inner stimulus ring that were slightly closer to the unrotated PC 2s in their respective subspaces. The projections associated with the inner stimulus ring are shown in magenta for all subjects in Fig. 6. The three projections onto the three outer ring subspaces for subjects 6 and 7, however were relatively near the unrotated PC 1s of the three outer ring subspaces.

The difference in $\phi_{i\,\max}$ across rings is likely at least partially attributable to differences in cortical folding in portions of cortex

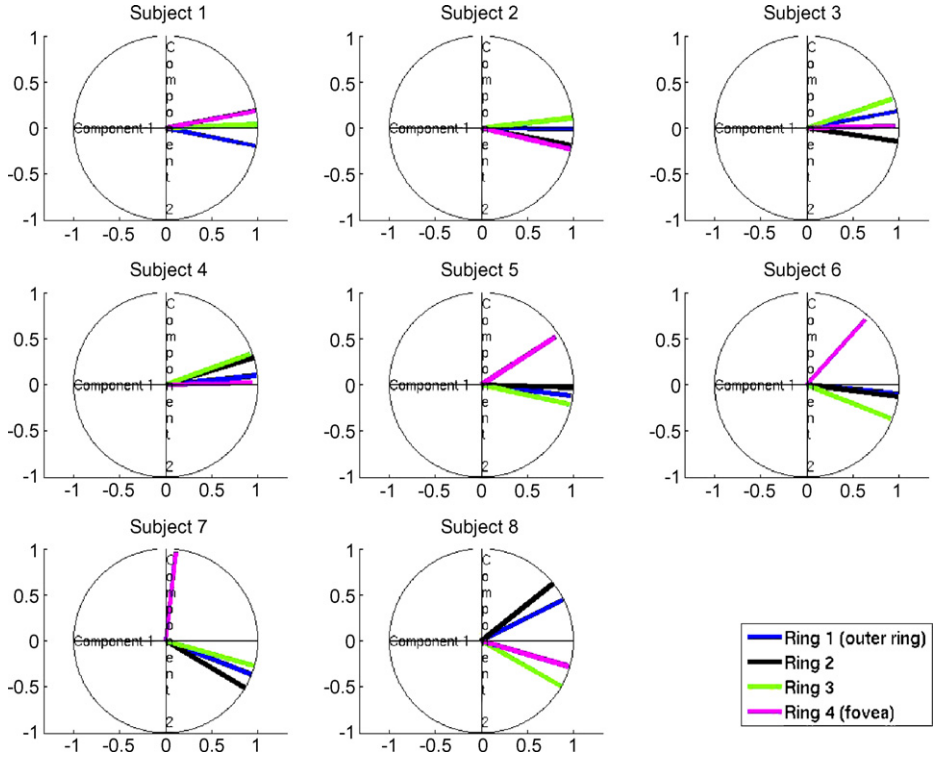

Fig. 6. Projections of intra-subject $C'(t, \theta_{\max})$ onto the individual ring subspaces of all subjects. Labeled 'Component 1' and 'Component 2' correspond to the PC 1 and PC 2 of each individual subject. Lengths and phases as shown within each individual subspace are drawn to scale. Unit circles are drawn to facilitate comparisons of projection lengths.

corresponding to different regions of the visual field. As has been discussed, differences in folding across the parts of cortex responsive to different regions of visual field are expected to result in a varying linear combination of sources associated with responses from each region. Another possible explanation for varying linear combinations of sources at different eccentricities within a single subject are differential contributions of the *M* and *P* pathways at different eccentricities (Baseler and Sutter, 1997).

The $\phi_{i\,\min}$ are listed in Table 4 with the $\phi_{i\,\max}$. It can be seen that the $\phi_{i\,\min}$ tended to be relatively close to the unrotated PC 2s for each ring subspace and the $\phi_{i\,\max}$ tended to be relatively close to the unrotated PC 1s in each individual ring subspace. This was to be expected as the PC 2 in the intra-subject composite and the PC 2s in the individual subspaces accounted for less variance than the PC 1s. The smaller amount of variance accounted for by PC 2 guaranteed that the region in each 2D subspace near the unrotated PC 2 was associated with the noisiest temporal processes in the subspace.

Fig. 7C is a plot of $I'_{\max}$ for each subject. The $I'_{\max}$ correspond to the time functions in individual subspaces at the locations of the projection of $C'(t, \theta_{\max})$ onto each individual subject subspace. One motivation for plotting each $I'_{\max}$ is to be able to visually inspect how similar the individual time functions are to each other at the rotations that bring the individual time functions closest together. Fig. 7A and B are plots of the unrotated temporal PC 1s and PC 2s for all subjects. Recall that subjects 6 and 7 displayed considerably different $\phi_{i\,\max}$ for the inner ring subspace than for the outer three ring subspaces. A considerable qualitative difference can therefore be observed in the unrotated PC 1 and 2 of the inner ring for these two subjects relative to the PCs for other rings (inner ring PCs shown in magenta in Fig. 7). For all subjects to varying degrees, it can be seen in Fig. 7 that the $I'_{\max}$ display considerably less intra-subject variability than the unrotated temporal waveforms shown in Fig. 7A and B. A possible explanation for the greater intra-subject variability of the raw PCs in Fig. 7 is that the raw PCs consist of some linear combination of sources unique to the portion of cortex associated with each stimulus ring. This unique linear combination of sources is largely dependent on the local geometry of cortex. By finding a $C'(t, \theta_{\max})$ for each subject that projects well onto all individual ring subspaces at the $I'_{\max}$ time functions, we

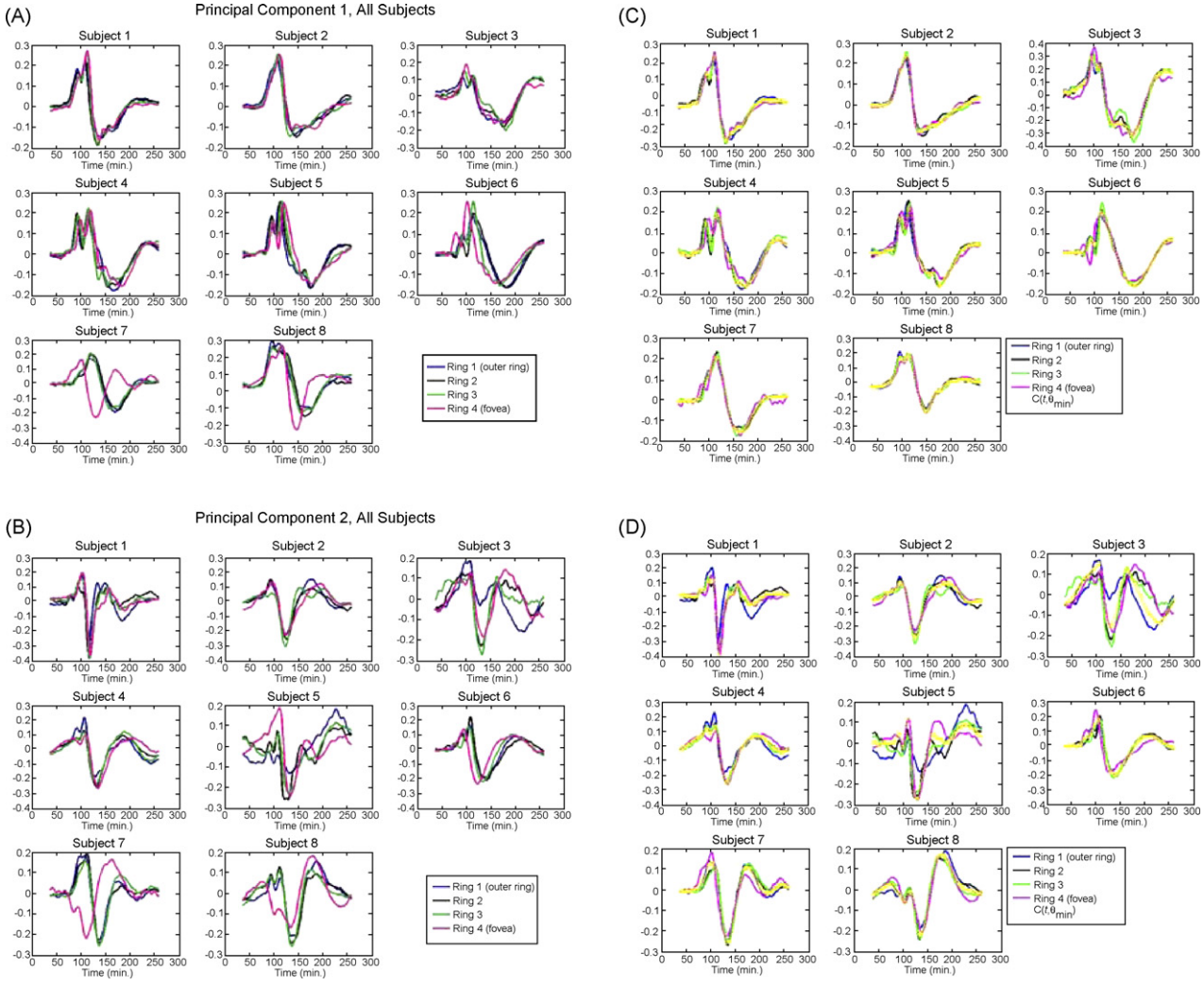

Fig. 7. (A) Principal component 1 for all rings for every subject. (B) Principal component 2 for all rings for every subject. (C) $I'_{\max}$ for all subjects and rings. Note that the waveforms in C show greater intra-subject similarity across rings than the waveforms in A and B. (D) $I'_{\min}$ for all subjects and rings.

have found temporal processes that display a significant amount of consistency across the visual field within a subject. This is exemplified by the substantial similarity of the I'_{max} waveforms shown in Fig. 7C.

Plots of I'_{min} for all subjects are shown in Fig. 7D. One hypothesis that could explain the relatively great intra-subject variability of the I'_{min} across the visual field (relative to the intra-subject variability of the I'_{max}) might be that the I'_{min} contain significant extrastriate contributions, perhaps associated with relatively weak, very small and/or deep regions of cortical activation (DeYoe et al., 1996). An alternative hypothesis/possible contributing factor that might explain the variations in the I'_{min} across the visual field for any given subject could be varying M and P contributions across the visual field (Dacey, 1993; Baseler and Sutter, 1997). Spatially specific attention and feedback effects have been observed in two prior mfVEP studies (Seiple et al., 2002; Slotnick et al., 2002). A third possible contributing factor, therefore, might be that some of the intra-subject differences might correspond to temporal processes involving feedback and/or attention that might be expected to vary at different regions of the visual field within the same subject.

3.3. Inter-subject results

Application of a SVD to a $V(s \times e \times p, t)$ matrix formed as described in Section 2.2 by concatenating signal windows from each subject appropriately into the $V(s \times e \times p, t)$ matrix resulted in the first two PCs accounting for 47% and 20% of the inter-subject variance, respectively. Fig. 8 is a plot of the percent variance accounted for by the first 17 inter-subject PCs for an inter-subject SVD done across the entire visual field.

The fact that two PCs accounted for the majority of inter-subject variance indicated that a "composite" 2D inter-subject subspace defined by the two dominant inter-subject temporal PCs accounted for the majority of the temporal variance in the $V(s, e, p, t)$ space.

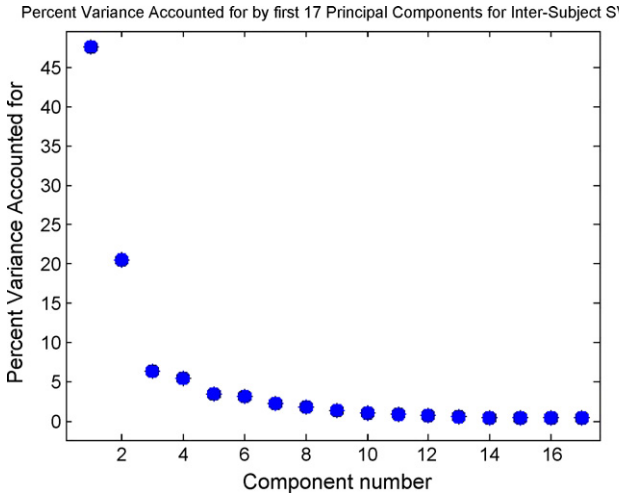

Fig. 8. Percent variance accounted for by the first 17 inter-subject temporal PCs.

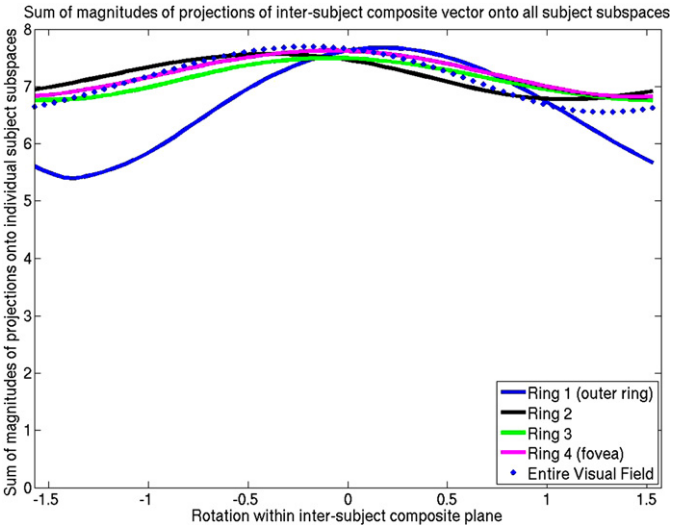

Fig. 9. $L(\theta)$ curves summed across subjects.

The first and second composite inter-subject temporal eigenvectors were determined for each ring of the stimulus separately. This was done by performing four SVDs on $V(s \times e \times p, t)$ matrices containing only the appropriate subset of patches corresponding to each stimulus ring from each subject. Each of the four 2D inter-subject ring-by-ring composites could then be compared to the corresponding ring-by-ring dominant two PCs as determined for each subject individually. A composite inter-subject 2D subspace for the entire visual field was determined by applying SVD to combined data from the entire visual field for all subjects. The inter-subject composite for the entire visual field was compared with each of the subspaces resulting from application of SVD to individual subject data from the entire visual field.

Fig. 9 is a plot of the $L(\theta)$ curves summed across all subjects for the inter-subject subspace comparisons done ring by ring. In Fig. 9, if all of the individual subspaces were identical to the inter-subject composite subspace, the sum of the lengths of the projections would sum to eight at all rotations within the composite subspace (sum of eight unit length vectors, one for each of eight subject subspaces). All of the $L(\theta)$ curves with the exception of the $L(\theta)$ curve associated with the outer ring of the stimulus displayed projection lengths that were consistently near one for all rotations. The maximum of the $L(\theta)$ curve for the outer ring of the stimulus is near 8, however the minimum point in the $L(\theta)$ curve for the outer ring deviated considerably from 8. This indicates that at least one of the sources contributing to the outer ring responses for the subjects did, as a whole, display substantial inter-subject similarity. Other source(s) contributing to the outer ring responses of the subjects, however, were significantly variable from subject to subject. A possible reason for the differing responses to the outer ring could be that it was not surrounded by other patches as was the case for all other stimulus rings.

Fig. 10 is a plot of the subject-by-subject $L(\theta)$ curves using an inter-subject composite as determined across the entire field. The lengths of projections were found by projecting rotations

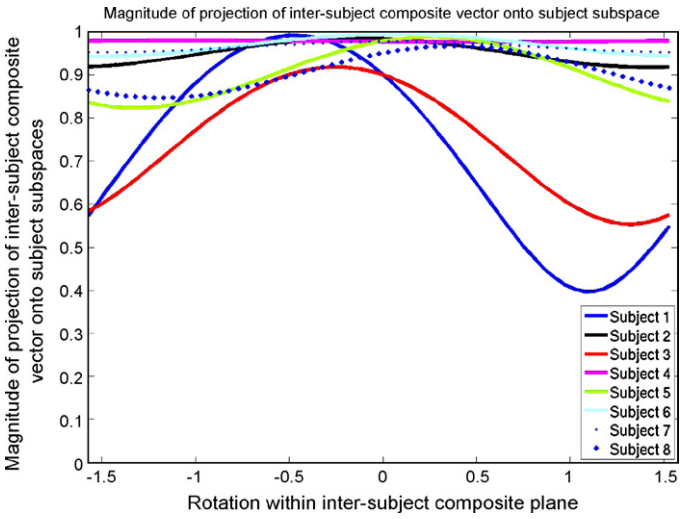

Fig. 10. Subject by subject $L(\theta)$ curves. Rotation in inter-subject composite subspace is specified relative to unrotated PC 1 in inter-subject composite subspace.

of the inter-subject composite onto individual subject subspaces that were derived from data from the entire visual field for each subject. It can be seen that all subjects except subjects 1 and 3 display projection lengths near one for all rotations in the composite plane. Note that the subjects who deviated from the inter-subject composite at some rotations in the composite plane nevertheless showed substantial similarity to the composite plane at other rotations. This could indicate that some sources were similar between subjects but not all sources showed significant inter-subject similarity.

$\theta_{\max}$ was determined at each ring across all individual subject subspaces as determined at each stimulus ring (four applications of Eq. (12) with $M = 8$). Eq. (12) was applied to determine the rotations in each of the four ring-by-ring inter-subject composite planes that maximized the sum of the lengths of the projection onto the individual subject subspaces for each ring (solving for one $\theta_{\max}$ for all subjects per stimulus ring). Table 5 contains the lengths of projection ($L(\theta_{\max})$) resulting from the projection of the inter-subject $C'(t, \theta_{\max})$ for each stimulus ring onto the eight individual subject subspaces as determined for the appropriate stimulus ring. The standard deviation of the $L(\theta_{\max})$ across stimulus rings was quite low for all subjects. This demonstrates that the relationship of the individual subspaces to the composite (and hence the $L(\theta_{\max})$ measure) is fairly consistent with varying stimulus eccentricity.

Similarly Eq. (13) was used to determine $\theta_{\min}$ at each ring using data from all of the individual subject subspaces corresponding to each stimulus ring (four applications of Eq. (13) with $M = 8$). The rotations in each of the four ring-by-ring inter-subject composite planes that minimized the sum of the lengths of the projection onto the individual subject subspaces for that ring were determined (solving for one $\theta_{\min}$ for all subjects for each stimulus ring). Table 5 contains $L(\theta_{\min})$, the lengths of projection when the $C'(t, \theta_{\min})$ for each stimulus ring was projected onto the eight individual subject subspaces as determined for the appropriate stimulus ring.

For most subjects, although the standard deviations of the $L(\theta_{\min})$ were higher than those associated with $L(\theta_{\max})$, the standard deviations were still relatively low. For subjects 3 and 5, however, the standard deviation of the $L(\theta_{\min})$ were relatively high with the associated projection lengths being relatively low. Subject 1 also exhibited uniformly low $L(\theta_{\min})$ across rings with relatively low standard deviation.

It can be seen that some of the $L(\theta_{\min})$ are relatively near one, but many of the $L(\theta_{\min})$ are substantially smaller than the $L(\theta_{\max})$. This indicates that the multiple subjects do share some temporal processes of substantial similarity (mainly the $I'_{\max}$) but there is a substantial tilt between the multiple subject subspaces at those portions of the subspaces that correspond to linear combinations of sources that are relatively dissimilar between subjects (the $I'_{\min}$). This is to be contrasted with the individual subject data which showed relatively great similarity in both the $I'_{\max}$ and $I'_{\min}$, indicating relatively little tilt between the intra-subject subspaces at every linear combination of sources in the intra-subject composite plane and therefore substantial intra-subject similarity in response across stimulus rings.

Table 6 lists the rotations within the individual subject subspaces, $\phi_{i\,\max}$, at the locations of projection of $C'(t, \theta_{\max})$ onto each individual subject subspace. It can be seen that most of the phases in Table 6 are closer to the unrotated PC 1 in each individual subject's subspace (defined as being at 0 phase within each individual subspace) than to the unrotated PC 2 in each individual's subspace. However, there is a considerable amount of deviation from the unrotated PC 1 across subjects.

Table 5
Lengths of projection of inter-subject composites $C'(t, \theta_{\max})$ and $C'(t, \theta_{\min})$ onto individual subject subspaces $L(\theta_{\max})$ and $L(\theta_{\min})$ and associated standard deviations across subjects and rings

Subject	Ring 1 $L(\theta_{\max})$	Ring 1 $L(\theta_{\min})$	Ring 2 $L(\theta_{\max})$	Ring 2 $L(\theta_{\min})$	Ring 3 $L(\theta_{\max})$	Ring 3 $L(\theta_{\min})$	Ring 4 $L(\theta_{\max})$	Ring 4 $L(\theta_{\min})$	S.D. $L(\theta_{\max})$	S.D. $L(\theta_{\min})$
S1	.925	.397	.955	.462	.902	.544	.973	.544	.032	.071
S2	.988	.899	.970	.899	.977	.865	.977	.939	.007	.030
S3	.933	.045	.920	.860	.819	.912	.959	.797	.061	.408
S4	.965	.871	.977	.968	.962	.953	.965	.934	.007	.043
S5	.971	.438	.920	.775	.945	.725	.953	.919	.021	.202
S6	.990	.931	.968	.960	.986	.939	.898	.926	.043	.015
S7	.959	.928	.935	.960	.945	.934	.980	.892	.019	.028
S8	.945	.883	.920	.893	.961	.885	.921	.867	.020	.011
$\theta_{\max}$ or $\theta_{\min}$	.175	−1.38	−0.387	1.08	−.0872	−1.55	−.0812	1.44	–	–

Table 6
Rotations in individual subspaces, $\phi_{i\,\max}$ and $\phi_{i\,\min}$, at locations of projection of inter-subject $C'(t, \theta_{\max})$ and $C'(t, \theta_{\min})$

Subject	Ring 1 $\phi_{i\,\max}$	Ring 1 $\phi_{i\,\min}$	Ring 2 $\phi_{i\,\max}$	Ring 2 $\phi_{i\,\min}$	Ring 3 $\phi_{i\,\max}$	Ring 3 $\phi_{i\,\min}$	Ring 4 $\phi_{i\,\max}$	Ring 4 $\phi_{i\,\min}$
S1	−.001	−.594	.230	−1.04	−.170	.888	.0630	1.55
S2	−.198	1.40	−.134	1.34	.355	−1.30	−.211	1.33
S3	.347	−1.46	−.369	1.19	.219	−1.15	−.360	1.32
S4	−.426	1.08	−.385	1.11	−.151	1.34	.646	−.866
S5	.091	−1.13	−.387	.765	−.407	.757	.982	−.505
S6	.689	−.845	−1.06	.374	.373	−1.07	−.040	1.41
S7	−.711	−.805	−1.06	.353	−.605	.789	−1.15	.437
S8	.206	−1.26	.687	−.749	−.357	1.05	−.313	1.48
$\theta_{\max}$ or $\theta_{\min}$	.175	−1.38	−.387	1.08	−.0872	−1.55	−.0812	1.44

The $\phi_{i\,\min}$ are also presented in Table 6. It can be seen that the $\phi_{i\,\min}$ are predominantly near the unrotated PC 2 in each individual subspace, but do exhibit some variation from the unrotated PC 2 across subjects.

Fig. 11 contains the inter-subject $\phi_{i\,\max}$ as determined for the entire visual field. The difference in $\phi_{i\,\max}$ across subjects exhibited in Fig. 11 (also apparent in Table 6 for data in which SVDs were performed ring-by-ring) is likely at least partially attributable to differences in cortical folding among subjects. As discussed, each subject has a unique cortical geometry leading to differences in the observed combination of sources for each subject.

Fig. 12C is a plot of the waveforms in the individual subject subspaces, $I'_{\max}$ at the rotation of the entire-visual field inter-subject composite $C'(t, \theta_{\max})$ maximizing the sum of the lengths of the projections onto all of the individual subspaces as determined across the entire visual field for each. Fig. 12A and B are plots of the unrotated PC 1s and PC 2s for all subjects. It can be seen that the $I'_{\max}$, display less inter-subject variability than the unmodified temporal PC 1s or PC 2s. A possible explanation for the greater variability of the raw PCs is that the raw PCs are likely influenced by the unique cortical folding pattern of each subject and therefore consist of some linear combination of sources unique to each subject. Finding an inter-subject $C'(t, \theta_{\max})$ for the entire visual field that projects well onto all individual subject subspaces allows us to compare similar linear combinations of sources in the individual subspaces. The $I'_{\max}$ waveforms for each subject shown in Fig. 12C therefore show a relatively more consistent temporal process for all subjects than the raw PCs.

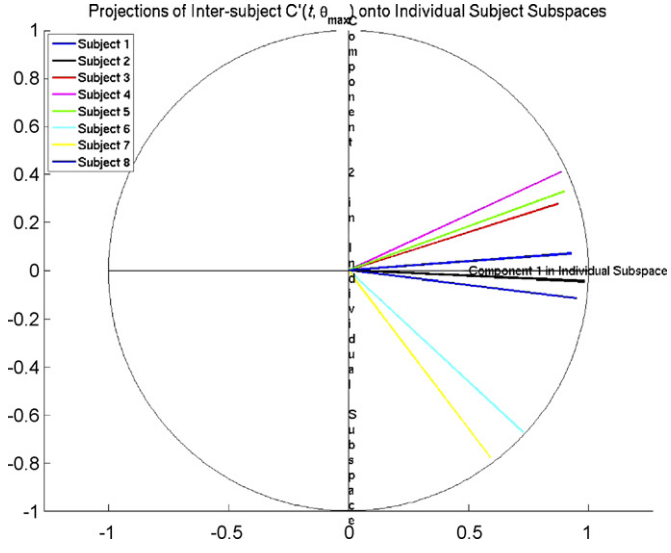

Fig. 11. $\phi_{i\,\max}$, or plots of projection of inter-subject $C'(t, \theta_{\max})$ (as determined from data from the entire visual field) onto individual subject subspaces (also determined from data from the entire visual field). Lengths and phases of the projections are drawn to scale. A unit circle is drawn to facilitate comparisons of projection lengths.

Fig. 12D is a plot of the temporal vectors in each of the individual subject subspaces, $I'_{\min}$, at the rotation corresponding to the location where the rotation of the entire visual field composite produced the minimum sum of lengths across projections onto individual subject subspaces. Although there are some similarities in the $I'_{\min}$, there are also a variety of inter-subject differences apparent in Fig. 12D.

As was the case for the intra-subject $C'(t, \theta_{\min})$ and $I'_{\min}$, the inter-subject $C'(t, \theta_{\min})$ and $I'_{\min}$ were, for the most part, closer to the unrotated PC 2 in the composite and individual subspaces. Therefore, much of the variability is likely due to the fact that $C'(t, \theta_{\min})$ and $I'_{\min}$ were derived from the noisiest portions of the subspaces. Reasons for the variability and noisiness at the $I'_{\min}$ rotations could be due to any combination of a number of factors. It is possible that the source or sources at the $C'(t, \theta_{\min})$ rotation consist of substantial extrastriate contributions that are relatively weak, small, and/or deep (DeYoe et al., 1996). Another possible explanation that could contribute to inter-subject differences in the $I'_{\min}$ (as well as the less extensive differences in $I'_{\max}$) could be individual differences in feedback and/or attention (Seiple et al., 2002; Slotnick et al., 2002).

4. Discussion

In addition to confirming the previously known finding that two PCs account for over 50% of intra-subject variance of the multifocal VEP (Maier et al., 1987; James, 2003; Zhang and Hood, 2004b; Carney et al., 2006) we have quantified inter-subject similarity of the mfVEP, finding that two dominant inter-subject composite PCs account for 67% of inter-subject variance.

It is important to note that temporal PCs determined via SVD are not necessarily physiologically meaningful (Maier et

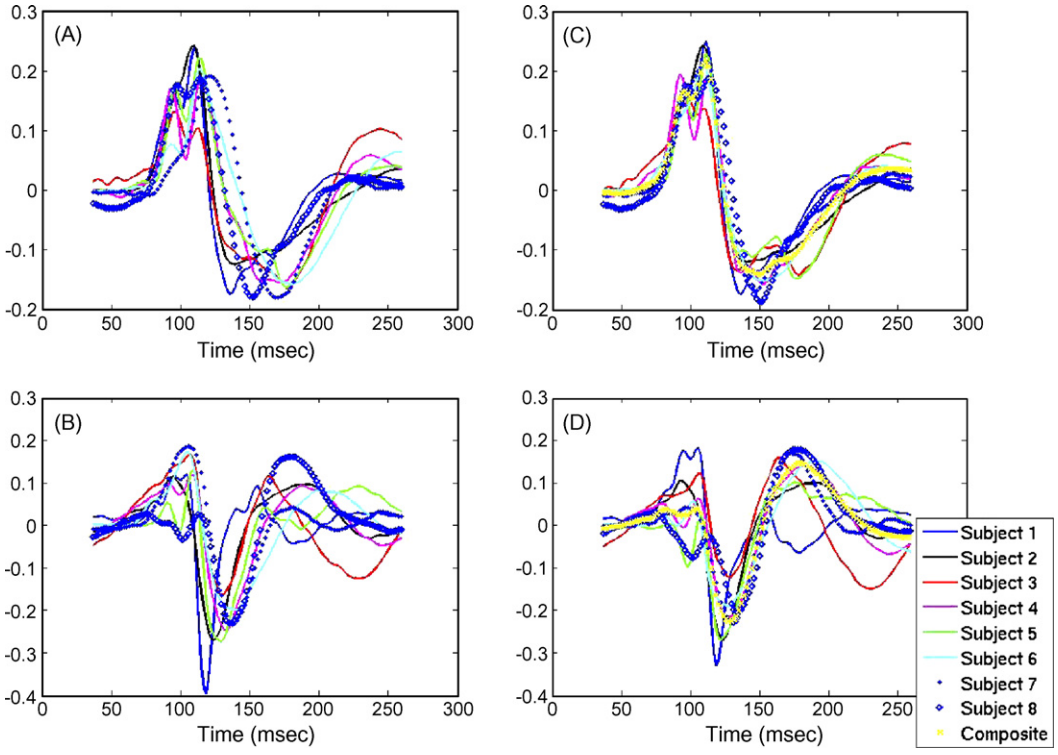

Fig. 12. (A) Unmodified PC 1s for all subjects. (B) Unmodified PC 2s for all subjects. (C) I'_{max} for all subjects. Note that the waveforms in C show greater inter-subject similarity than those in A and B. (D) I'_{min} for all subjects.

al., 1987; Bartels and Zeki, 2004). SVD decomposes data into orthogonal spatial and temporal components. The orthogonality constraint is an artificial one; the underlying physiological time functions are most probably not orthogonal. Therefore, the composite 2D intra- and inter-subject temporal subspaces that we use in comparisons are not necessarily physiologically meaningful. However, the composites can be used as fixed standards to which inter- and intra-subject temporal data are compared to gauge variability. We use the composites to facilitate alignment of corresponding temporal features.

One argument against rotating the principal temporal components derived from mfVEP data into alignment prior to combining or comparing inter- or intra-subject data is that perhaps the unrotated principal component 1 is already a physiologically meaningful source (Zhang and Hood, 2004b). In Zhang et al., the authors suggested that PC 1 likely is a "relatively pure V1 component and can be used to study the processing in V1." One aspect of the authors' arguments is based on the observation that the spatial topographies associated with PC 1 display a flip in polarity between the upper and lower visual fields. In our inter- and intra-subject analyses, we derived temporal 2D subspaces from various subsets of individual and inter-subject data and have shown that corresponding temporal features in these subspaces are at variable rotations in each individual subspace. For example, we found that the rotation in each individual subspace, $\phi_{i\,max}$, at the location of the projection of the composite rotation, $C'(t, \theta_{max})$, varied substantially within individual subjects and between individual subjects (see Figs. 7 and 11). Much of the variability observed is likely due to the unique cortical folding of the cortical region or regions from which each individual subspace was derived. Cortical folding is expected to cause the observed linear combination of sources at any given rotation in each individual subspace to be variable from one individual subspace to another. Our results therefore indicate that the temporal waveform associated with the unrotated PC 1 as determined from a single or only a few subjects is likely some unknown superposition of sources that is likely dependent on the unique cortical folding associated with the brain regions from which the PC is derived. It therefore seems unlikely that the unrotated PC 1 (at least as determined from a single or a few subjects) can be used to reliably isolate V1 temporal activity. However, perhaps only minimal distortions of PC time functions are to be expected in a situation such as the experiments described in Zhang and Hood (2004b) in which PCs from a relatively great number of subjects (greater than 30 in the case of Zhang et al.) are averaged. In a case such as this, perhaps individual variations in temporal data that are attributable to cortical geometry differences will tend to cancel out.

Our finding that there is generally excellent agreement of the 2D subspaces across eight subjects (recall that there was a minor reduction of variance from 73% to 67% of variance accounted for) implies that there is significant commonality of the temporal responses across our subjects. This likely implies that there is significant similarity in V1 time functions across subjects, assuming (as evidence indicates in Fortune and Hood, 2003) that there are sizable contributions of striate generators to the mfVEP. If V1 time functions are substantially different across subjects, then there may be some other principle, not yet understood, that underlies the observed subspace similarity across subjects.

If future work involving source localization reveals that the underlying V1 time function is essentially the same across subjects, this could suggest useful extensions of the methods presented in this paper. A 'composite V1 time function' could be defined based on the expected temporal response of V1 obtained from source localization of multiple subjects. To obtain an estimate of the V1 time function from the multifocal data of a new subject, one could rotate within the 2D subspace defined by PC 1 and 2 of the new subject to best match the composite V1 time function. The electrode weightings and time functions obtained from multifocal data could be used to facilitate isolation of the V1 components in non-multifocal experiments.

Many EP studies rely on comparison of averaged, raw temporal waveforms across subjects. As discussed in (Baseler et al., 1994), averaging of data from multiple subjects (or, as our data suggests, even averaging data from different regions of the visual field for a single subject) can result in unintended signal cancellation and distortion due to individual differences in cortical folding. As shown in Figs. 7 and 12, examination of comparable linear combinations of sources rather than comparisons of raw data or comparisons of unrotated temporal PCs can mitigate much apparent intra- and inter-subject variability that is presumably largely due to individual differences in cortical geometry. The alignment process that we propose might therefore facilitate investigation of neural processes of interest by disambiguating such processes from differences that are more likely due to cortical geometry variability.

Acknowledgements

This work was supported by NIH EY015825 and NIH T32 EY07.

Appendix A

A.1. Cortical folding and the rotation problem

Consider three sets of $V_k(e, t)$ data, with the subscript k representing the three datasets. The voltage for a single a single patch can be written as

$$V_k(e, t) \cong \sum_{c=1}^{2} E_k(e, c)T(c, t) \tag{A.1}$$

Each of the datasets is associated with the same pair of time functions, $T(1, t)$ and $T(2, t)$. The two time functions can be arbitrary other than having unit norm and being orthogonal to each other. For simplicity we consider the case with just two electrodes ($e = 1$ or 2) where the first component is the same for all three datasets:

$$E_k(e, 1) = [1\ 0]$$

The second components for the three datasets are chosen to be very slightly different from each other:

$$E_1(e, 2) = [0\ .999], \qquad E_2(e, 2) = [0\ 1.001],$$
$$E_3(e, 2) = [.001\ 0\ .999]$$

A singular value decomposition of $V_k(e, t)$ gives:

$$[U_k, S_k, \mathrm{PC}_k] = \mathrm{SVD}(V_k)$$

where the new time functions are rotated versions of the original time function:

$$\mathrm{PC}_k(1, t) = \cos(\theta_k)T(1, t) + \sin(\theta_k)T(2, t),$$
$$\mathrm{PC}_k(2, t) = -\sin(\theta_k)T(1, t) + \cos(\theta_k)T(2, t)$$

where $\theta_1 = 0^\circ$, $\theta_2 = 90^\circ$, and $\theta_3 = -58^\circ$.

That is the two PCs for the first example, with $\theta_1 = 0$, are identical to the original time functions. The two PCs for the second example with $\theta_2 = 90^\circ$ are identical to the original time functions except in reverse order and with a sign flip of one of the components. For the third example, because of the slight non-orthogonality of the two electrode weightings the two principal components are rotated by -58° from the original components.

We like this example because it is remarkable that an amazingly small change in the electrode weighting can make a large change in the principal component time functions that are obtained from the SVD algorithm. The reason for the dramatic jump from 0 to $\pi/2$ for $k = 1$ and 2 is because in the former case the time function, $T(1, t)$ is associated with the slightly stronger electrode function and in the latter case it is associated with the slightly weaker electrode weighting. Since SVD sorts the principal components according to the amount of variance accounted for there is a switch in components in going from case 1 to case 2. This example provides a vivid demonstration that the time functions can be very sensitive to the electrode weightings.

A.2. SSE derivation of ϕ_{irot}

In Section 2.6, we show how, given any rotation in the composite subspace, the closest rotation in an individual subspace can be found by projecting the composite vector onto the individual subspace and determining the phase of the projection within the individual subspace (see Eq. (11)). An alternative to the geometric derivation in Section 2.6 is one that uses SSE to obtain the same result.

The distance between a rotated time function within the composite space and a rotated time function in the mth individual subspace is given by the sum of squared differences between the two:

$$\mathrm{SSE}(\theta, \phi_i) = \sum_{t=1}^{N} (C'(t, \theta) - I'_m(t, \phi_i))^2 \tag{A.2}$$

where $I'_m(t, \phi_i)$ can be written as (Eq. (6)):

$$I'_m(t, \phi_i) = I_m(1, t)\cos(\phi_i) + I_m(2, t)\sin(\phi_i)$$

We will fix θ in order to find the angle in the individual subspace, ϕ_{irot}, that minimizes the sum of square error in Eq. (A.2). It is useful to first define the projection of $C'(t, \theta)$ onto an individual subspace (Eq. (9)):

$$P(\theta, c) = \sum_{t=1}^{N} C'(t, \theta) \times I(c, t)$$

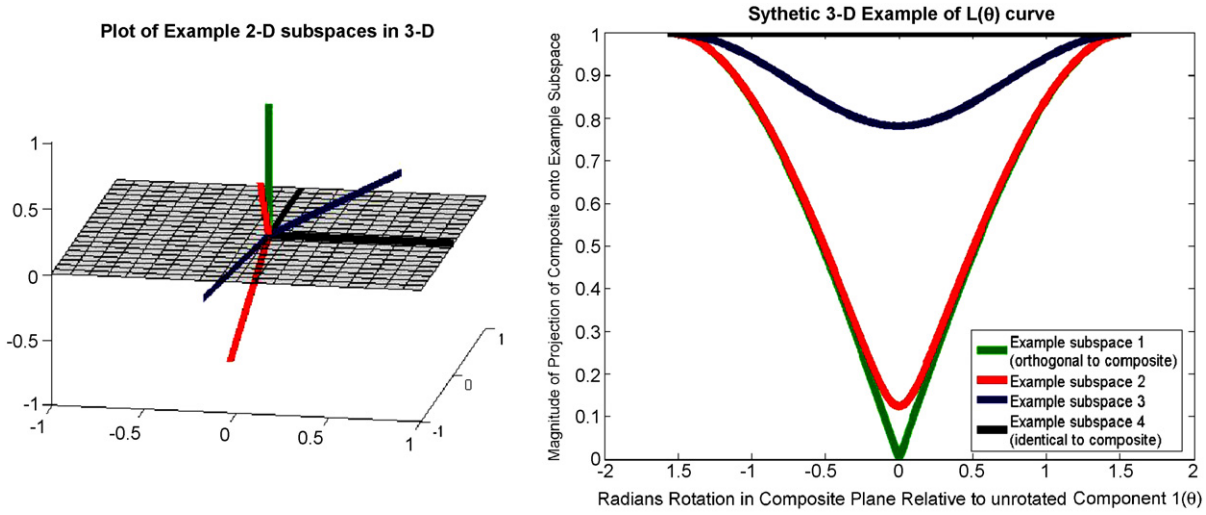

Fig. A.1. Left: four pairs of principal components defining four 2D subspaces in 3D. The composite subspace to which all four the individual subspaces are compared is shaded in gray. Right: corresponding $L(\theta)$ plots for the example 2D subspaces shown.

Combining Eqs. (6), (A.2) and (9) gives:

$$\mathrm{SSE}(\theta, \phi_i) = 2 - 2(\cos(\phi_i)P(\theta, 1) + \sin(\phi_i)P(\theta, 2)) \quad \text{(A.3)}$$

The minimum (or maximum) value of Eq. (A.3) is obtained by taking the derivative of Eq. (A.3) with respect to ϕ_i. The angle of interest in the individual subspace, ϕ_{irot}, is therefore:

$$\phi_{\mathrm{irot}} = a\tan\left(\frac{P(\theta, 2)}{P(\theta, 1)}\right) \quad \text{(A.4)}$$

The above equation is equivalent to Eq. (11) in Section 2.6.

A.3. Three-dimensional example of $L(\theta)$ plot

For each individual subspace, we can find the lengths of the projections of rotations in the composite plane onto the individual subspace as a function of rotation angle within the composite plane, θ, by using Eq. (10).

Examination of this plot for each individual subspace can give us information about the tilt between each individual subspace and the composite subspace for all of the linear combinations of the two composite subspace temporal waveforms (i.e. for every θ). In Section 3, we present intra- and inter-subject $L(\theta)$ plots. In this section, we will present $L(\theta)$ plots for several example 2D subspaces in 3D to acquaint the reader with interpretation of the plots.

Fig. A.1 (left) contains plots of four 2D subspaces embedded in 3D with different alignments relative to the composite subspace $\left(\begin{bmatrix}1 & 0 & 0\\ 0 & 1 & 0\end{bmatrix}^{\mathrm{T}}\right)$. Fig. A.1 (right) is a plot of the corresponding $L(\theta)$ plots for each of the four alignments.

The $L(\theta)$ plot shown in black corresponds to a subspace that is perfectly aligned with the composite subspace. It can be seen that for all rotation angles within the composite subspace, θ, ranging from $-\pi/2$ to $\pi/2$ the associated rotated vector in the composite subspace, $C'(t, \theta)$, projects onto the individual subspace shown in black with length of 1. The example individual subspace shown in green $\left(\begin{bmatrix}1 & 0 & 0\\ 0 & 0 & 1\end{bmatrix}^{\mathrm{T}}\right)$ is orthogonal to the composite subspace in one dimension but intersects the composite subspace in the other dimension. The $L(\theta)$ curve for the green individual subspace therefore starts off at 1 at the $C'(t, \theta)$ that intersects with the individual subspace and rapidly drops to 0 at the rotation $C'(t, \theta)$ that is completely orthogonal to the green individual subspace. The individual subspace shown in blue $\left(\begin{bmatrix}-0.1824 & -0.9723 & -0.1460\\ 0.759 & -0.2336 & 0.6077\end{bmatrix}^{\mathrm{T}}\right)$ has a moderate amount of tilt relative to the composite subspace while the subspace shown in red $\left(\begin{bmatrix}-0.0915 & -0.6748 & -0.7323\\ 0.0837 & -0.7380 & 0.6696\end{bmatrix}^{\mathrm{T}}\right)$ displays more extreme tilt relative to the composite than the blue subspace. The $L(\theta)$ curve associated with the blue subspace therefore displays a greater projection length at the rotation producing maximum tilt away from the composite subspace than the curve associated with the red subspace does.

An important difference between our N-dimensional temporal data and the three dimensional example shown in Fig. A.1 is that for 2D subspaces in 3D there will be at least one rotation in the composite plane that projects onto an individual subspace with projection length of unity. In situations in which 2D subspaces are embedded in higher dimensions than three, the 2D subspaces do not necessarily have to be coplanar at any rotation and therefore the $L(\theta)$ plots do not have to have maxima equal to 1.

References

Bartels A, Zeki S. The chronoarchitecture of the cerebral cortex. Philos Trans R Soc 2004;360:733–50.

Baseler HA, Sutter EE. M and P components of the VEP and their visual field distribution. Vision Res 1997;37:675–90.

Baseler HA, Sutter EE, Klein SA, Carney T. The topography of visual evoked response properties across the visual field. Electroencephalogr Clin Neurophysiol 1994;90:65–81.

Carney T, Ales J, Klein SA. Advances in multifocal methods for imaging human brain activity. Proc SPIE 2006;6057:16.1–12.

Dacey DM. The mosaic of midget ganglion cells in the human retina. J Neurosci 1993;13:5334–55.

DeYoe EA, Carman GJ, Bandettini P, Glickman S, Wieser J, Cox R, et al. Mapping striate and extrastriate visual areas in human cerebral cortex. Proc Natl Acad Sci 1996;93:2382–6.

Engel SA, Glover GH, Wandell B. Retinotopic organization in human visual cortex and the spatial precision of functional MRI. Cereb Cortex 1997;7:181–92.

Foxe JJ, Simpson GV. Flow of activation from V1 to frontal cortex in humans a framework for defining "early" visual processing. Exp Brain Res 2002;142:139–50.

Fortune B, Hood DC. Conventional pattern-reversal VEPs are not equivalent to summed multifocal VEPs. Invest Ophthalmol Visual Sci 2003;44:1364–75.

James AC. The pattern-pulse multifocal visual evoked potential. Invest Ophthalmol Visual Sci 2003;44:879–90.

Maier J, Dagniele G, Sperkerijse J, van Dijk BW. Principal components analysis for source localization of VEPs in man. Vision Res 1987;27:165–77.

Seiple W, Greenstein VC, Holopigian K, Zhang X. The spatial distribution of selective attention assessed using the multifocal visual evoked potential. Vision Res 2002;42:1513–21.

Slotnick SD, Hopfinger JB, Klein SA, Sutter EE. Darkness beyond the light: attentional inhibition surrounding the classic spotlight. Neuroreport 2002;13:773–8.

Slotnick SD, Klein SA, Carney T, Sutter EE, Dastmalchi S. Using multi-stimulus VEP source localization to obtain a retinotopic map of human primary visual cortex. Clin Neurophysiol 1999;110:1793–800.

Sutter EE. The fast *m*-transform: a fast computation of cross correlations with binary *m*-sequences. SIAM J Comput 1991;20:686–94.

Zhang X, Hood DC. Increasing the sensitivity of the multifocal visual evoked potential (mfVEP) technique: incorporating information from higher order kernels using a principal component analysis method. Doc Opthalmol 2004a;108:211–22.

Zhang X, Hood DC. A principal component analysis of multifocal pattern reversal VEP. J Vision 2004b;4:32–43.